Large-Area PEDOT:PSS/c-Si Heterojunction Solar Cells With Screen-Printed Metal Contacts

Article · February 2018

DOI: 10.1002/solr.201700191

7 authors, including:

Dimitri Zielke
Laseroptik
29 PUBLICATIONS **794** CITATIONS
SEE PROFILE

Ralf Gogolin
Institute for Solar Energy Research (ISFH)
19 PUBLICATIONS **181** CITATIONS
SEE PROFILE

Marc-Uwe Halbich
Institute for Solar Energy Research (ISFH)
9 PUBLICATIONS **36** CITATIONS
SEE PROFILE

Wilfried Lövenich
Heraeus Holding
30 PUBLICATIONS **502** CITATIONS
SEE PROFILE

Large-Area PEDOT:PSS/c-Si Heterojunction Solar Cells With Screen-Printed Metal Contacts

*Dimitri Zielke, Ralf Gogolin, Marc-Uwe Halbich, Cornelia Marquardt, Wilfried Lövenich, Rüdiger Sauer, and Jan Schmidt**

A large-area BackPEDOT solar cell with a phosphorus-diffused emitter and a high-temperature-fired screen-printed Ag grid on the front surface and PEDOT:PSS as hole-collecting and passivating layer at the cell rear is developed. As base material, $15.6 \times 15.6\,cm^2$ pseudo-square industrial-type boron-doped *p*-type Czochralski-grown silicon wafers are used. The set-peak firing temperature (T_{set}) is varied from 850 to 870 °C with a total number of 32 processed solar cells. The optimum T_{set} of 870 °C results in a median solar cell efficiency of 19.0%. The best large-area BackPEDOT solar cell achieves an efficiency of 20.2%. Based on external quantum efficiency measurements, a rear surface recombination velocity $S_{rear} < 70\,cm\,s^{-1}$ is determined, a value which is on a par with today's industrial high-efficiency solar cells. Furthermore, a low-temperature metal paste is introduced, which is shown to be capable of metalizing the PEDOT:PSS-covered rear surface of the solar cells without damaging the rear surface passivation. The principle feasibility of such a rear metallization scheme is demonstrated. The parasitic absorption of infrared light within the PEDOT:PSS layer is identified as the major loss mechanism in the current cells, which might be overcome in the future by adding infrared-transparent additives to the PEDOT:PSS dispersion.

1. Introduction

Today, the photovoltaics industry is in technological transition from the aluminum "back-surface-field" solar cell (Al-BSF) toward the passivated emitter and rear solar cell (PERC).[1] The increased efficiency of the PERC solar cells compared to the Al-BSF solar cells is largely due to the reduced recombination at the rear surface. However, the excellent rear surface passivation of a PERC solar cell requires technologically advanced deposition of dielectric passivation layers, such as an AlO_x layer plus an additional SiN_y capping-layer, as well as a partial laser ablation, the so-called "laser contact opening" (LCO) of the dielectric stack. Those additional process steps increase the process complexity and thus the fabrication costs. An alternative approach for the rear surface passivation of a silicon solar cell is the deposition of the hole-selective polymer poly(3,4-ethylene-dioxythiophene):polystyrenesulfonate (PEDOT:PSS).[2] PEDOT:PSS serves as an effective rear surface passivation layer (as demonstrated by very low measured saturation current densities $J_0 < 50\,fA\,cm^{-2}$[3]) and, in addition, is well conductive for holes, thus, making the AlO_x/SiN_y rear surface passivation stack as well as the LCO step both obsolete, leading to a simplification of the overall process sequence.

PEDOT:PSS/silicon heterojunction solar cells received an increased interest since the pioneering works of Avasthi et al.[4] and He et al.[5] So far, the research has been focusing on the modification of the PEDOT:PSS dispersions with components such as graphene oxide[6,7] or zonyl[8] and investigations of the PEDOT:PSS/silicon interface.[9–11] Several groups improved the passivation of the rear surface of the solar cells[12–16] while the front surface was covered by PEDOT:PSS. Furthermore, fundamental properties of the silicon/PEDOT:PSS interface were studied[17–19] and investigations of the long-term stability of silicon/PEDOT:PSS solar cells[15,20,21] have been conducted. However, in the vast majority of published results, the PEDOT:PSS has been implemented on the front surface of this heterojunction silicon solar cells. In our previous work, we demonstrated that the application of the PEDOT:PSS on the front surface of a solar cell is insufficient for high-efficiency (>20%) applications, due to the high parasitic light absorption within the PEDOT:PSS layer.[2] In addition, in our previous work based on PEDOT:PSS/c-Si lifetime samples, we were able to demonstrate that implied open-circuit voltages $V_{oc.impl} > 700\,mV$ are achievable with PEDOT:PSS/c-Si junctions on non-textured planar silicon surfaces.[22] More recently, we were in fact able to reach an open-circuit V_{oc} of 688 mV by implementing a phosphorus-doped a-Si:H on the front and

Dr. D. Zielke, Dr. R. Gogolin, M. U. Halbich, C. Marquardt, Prof. J. Schmidt
Institute for Solar Energy Research Hamelin (ISFH)
Am Ohrberg 1, 31860 Emmerthal, Germany
E-mail: j.schmidt@isfh.de

Dr. W. Lövenich, Dr. R. Sauer
Heraeus Deutschland GmbH CoKG
HEB-EC, Chempark Leverkusen
51368 Leverkusen, Germany

Prof. J. Schmidt
Department of Solar Energy
Institute of Solid-State Physics
Leibniz Universität Hannover
Appelstr. 2, 30167 Hannover, Germany

DOI: 10.1002/solr.201700191

PEDOT:PSS on the rear surface of a c-Si solar cell,[23] demonstrating the enormous potential of the PEDOT:PSS for the application to high-efficiency heterojunction solar cells. With our proposed BackPEDOT concept[2] – which applies the hole-selective PEDOT:PSS to the planar rear surface of a solar cell – we were able to achieve a record-high efficiency of 20.6% on a laboratory-type solar cell with an area of (2×2) cm^2[3] using highest-purity float-zone silicon material and evaporated metal contacts at the front and the rear. In our approach presented here, we implement PEDOT:PSS as hole-collecting rear surface passivation layer to an industrial-type large-area silicon solar cell using Czochralski-grown silicon wafers and screen-printed front contacts. The aim is to implement the PEDOT:PSS material into an industrial-type state-of-the-art cell process.

2. Results and Discussion

2.1. BackPEDOT Solar Cells With Ag-Evaporated Rear Metallization

Figure 1 shows the process sequence of the developed industrial-type BackPEDOT cell process. **Table 1** shows median solar cell parameters and the parameters of the best solar cells for each set-peak temperature T_{set}. As best solar cells we define the cells with the highest measured energy conversion efficiencies for each particular set-peak temperature. The champion solar cell is the cell with the highest measured energy conversion efficiency in this work.

The median J_{sc} values of 38 ± 0.2 mA cm^{-2} are comparable for all set-peak temperatures T_{set}. The moderate J_{sc} values of our BackPEDOT cells are mainly due to parasitic absorption within the PEDOT:PSS layer, which will be discussed below in more detail.

The maximum median V_{oc} value of 648 mV is achieved at a T_{set} of 860 °C. At $T_{set} = 870$ °C the median V_{oc} decreases to a value of 643 mV. For each experimental setup, there is an optimal thermal budget for the activation of the passivation of the SiN_x layer on top of the n^+ emitter. Exceeding this thermal budget reduces the passivation quality and therefore the V_{oc}.

The median FF increases from FF = 77.8% at $T_{set} = 850$ °C to FF = 78.7% at $T_{set} = 870$ °C. The increase in FF is due to a decrease in the median series resistance R_s. The median R_s reduces from 0.97 Ω cm^2 at $T_{set} = 850$ °C to 0.79 Ω cm^2 at $T_{set} = 870$ °C. The decreasing R_s value with increasing T_{set} is caused by an improved contact formation between the Ag grid and the n^+ emitter at the front surface.

Highest efficiencies of 19.9% and 20.2% are achieved in each group at $T_{set} = 860$ °C and $T_{set} = 870$ °C, respectively. We observe a gap between the median efficiencies and the best efficiencies in each group of ~1%$_{abs}$. We attribute the relatively large scatter among the solar cell parameters to the largely manual handling of our novel process sequence and hence assume that an automated processing would strongly decrease the scatter.

2.2. Solar Cell Parameters of the Champion Solar Cell

Figure 2(a) shows a photograph of the front side of our champion large-area BackPEDOT solar cell with a

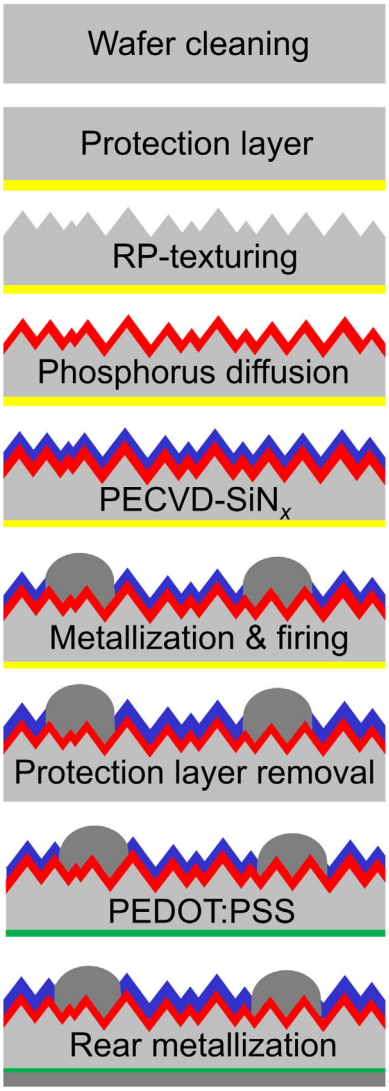

Figure 1. Schematic of the process flow of our industrial-type 15.6 × 15.6 cm^2 BackPEDOT solar cell.

15.6 × 15.6 cm^2 Cz-Si wafer used as base material. The photograph shows the dimension and the five bus-bar front Ag grid. Figure 2(b) shows the illuminated J–V curve (red symbols) and J_{sc}–V_{oc} curve (blue symbols) of the solar cell with the corresponding solar cell parameters in the insert. Our best large-area BackPEDOT solar cell achieves a short-circuit current density J_{sc} of 38.7 mA cm^{-2} and an open-circuit voltage V_{oc} of 656 mV. The low series resistance R_s of 0.63 Ω cm^2 indicates the good hole transport across the PEDOT:PSS/c-Si junction on the large area, leading to a fill factor FF of 79.5% and an efficiency of 20.2%.

Figure 3(a) shows an electroluminescence (EL) image of the solar cell shown in Figure 2(a). Notably, we do not observe any inhomogeneity caused by the PEDOT:PSS deposition. The dark rings in the EL image are caused by bulk defects within the Czochralski-grown silicon material and are not related to the PEDOT:PSS rear passivation. Figure 3(b) shows the measured

Table 1. Measured solar cell parameters as a function of the set-peak firing temperature.

Set-peak temperature T_{set}	J_{sc} [mA cm^{-2}]	V_{oc} [mV]	FF [%]	η [%]	pFF [%]	R_s [Ω cm^2]
850 °C best solar cell	37.4	645	78.8	19.0	82.3	0.73
850 °C median (4 cells)	37.8	646	77.8	18.9	82.5	0.97
860 °C best solar cell	38.5	645	79.9	19.9	83.1	0.62
860 °C median (18 cells)	37.8	648	78.4	19.0	81.9	0.69
870 °C best solar cell	38.7	656	79.5	20.2	82.5	0.63
870 °C median (10 cells)	38.2	643	78.7	19.2	82.0	0.79

Illuminated J–V and J_{sc}–V_{oc} measurements were performed at standard testing conditions (25 °C and illumination intensity of 100 mW cm^{-2}).

(red symbols) internal quantum efficiency (IQE) and reflectance of the champion solar cell. The minimum of the reflection curve R_{min} is set at 0%, to eliminate the influence of the front Ag grid shadowing. As a result the effective metallization fraction of 2.5% is calculated. The measurements have been performed on an area of 2×2 cm^2 marked by a red square in the EL-image shown in Figure 3(a). By fitting the IQE (black line) and performing a confidence plot (using our in-house developed software SCAN[24,25]), we determine the rear surface recombination velocity to be $S_{rear} < 70$ cm s^{-1} and the diffusion length in the bulk to be $L_b > 620$ µm. Those values are comparable to a standard PERC solar cell.[26,27] By fitting the reflectance data, we extract a rear surface reflectance fraction of only $R_b = 72\%$. This R_b value is $\sim 20\%_{abs}$ lower compared to a standard PERC solar cell.[26,27] The reason for the lower reflectance is the parasitic absorption of the PEDOT:PSS in the infrared wavelengths range, leading to only moderate J_{sc} values (see Table 1). One possibility to reduce the parasitic absorption is the incorporation of non-absorbing agents into the PEDOT:PSS dispersion. We currently examine the impact of several infrared-transparent agents into the PEDOT:PSS dispersion in our lab, with first results on large-area cells achieving already J_{sc} improvements of up to 1 mA cm^{-2} compared to our champion cell. Our first results indicate that the improvement of the optical properties of the PEDOT:PSS is a highly promising path toward future efficiencies >21% based on the BackPEDOT concept.

2.3. BackPEDOT Solar Cells With Screen-Printed Rear Metallization

The silver evaporation on the rear surface is one major obstacle toward an industrial feasibility of the large-area BackPEDOT solar cell. In the photovoltaics industry, the metallization is typically realized by screen-printing of a Ag paste through a screen on the front and a full-area Al paste on the rear surface of a solar cell. For a successful application of screen-printing onto the PEDOT:PSS surface, the paste has to fulfill the following criteria: 1) drying at low temperatures (<130 °C) must be possible, and 2) the solvent and/or other chemical components of the paste should not dissolve the underlying PEDOT:PSS layer. To fulfill both criteria, we have designed a novel low-temperature metal paste.

Table 2 compares the measured solar cell parameters of our solar cells metallized with evaporated silver and the new low-temperature metal paste.

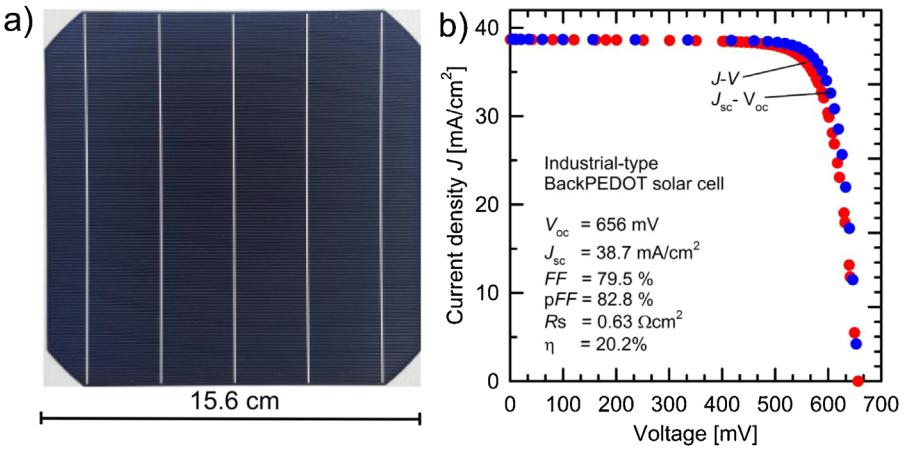

Figure 2. a) Photograph of the front side of the champion large-area BackPEDOT solar cell. b) Illuminated J–V curve (red symbols) and J_{sc}–V_{oc} curve (blue symbols) of the champion solar cell with the corresponding solar cell parameters in the insert.

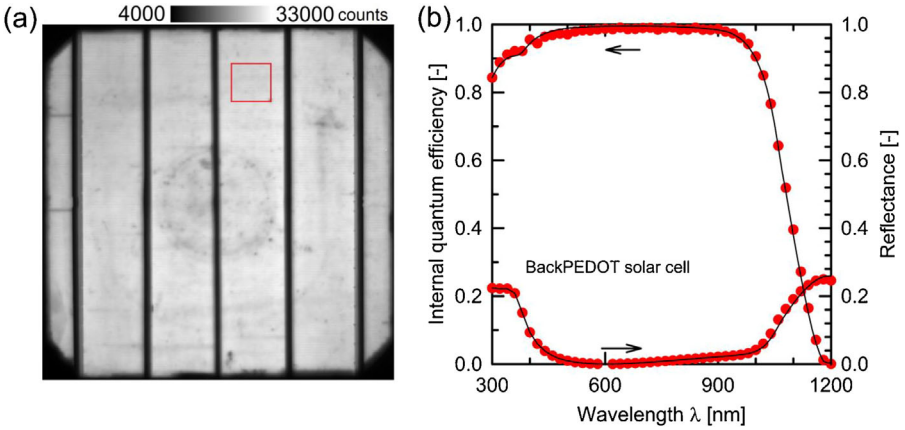

Figure 3. a) Electroluminescence (EL) image of the best $15.6 \times 15.6\,cm^2$ large BackPEDOT solar cell recorded at an applied voltage of 651 mV; (b) measured (red symbols) internal quantum efficiency and reflectance of the best solar cell. The measurements have been performed on an area of $2 \times 2\,cm^2$ marked by a red square in the EL-image of **Figure 3**(a). Fits to the measurements are shown as black lines.

The J_{sc} values are comparable for all solar cells and are in the J_{sc} range between 36.1 and 36.9 mA cm^{-2}.

The V_{oc} values are in average 7 mV higher for the solar cells with our low-temperature paste metallization. The highest V_{oc} value of 644 mV is measured on the solar cell metallized with the newly developed low-temperature paste, demonstrating that the passivation quality is not deteriorated by the implementation of the low-temperature metal paste into our BackPEDOT fabrication sequence.

The average R_s values are 1.95 and 2.3 Ω cm^2 for the solar cells with evaporated silver and paste metallization, respectively. The R_s values are slightly larger for the paste-metallized solar cells compared to the cells with evaporated Ag at the rear.

The larger R_s value for the paste metallization can – at least partly – be attributed to the morphology of the rear metal layer. **Figure 4**(a) shows scanning electron microscope (SEM) images of the PEDOT:PSS/silicon interface. The lower SEM image shows the cross section of the PEDOT:PSS/silicon interface. In the SEM image we observe voids within the metal layer. The thickness of the metal layer is ∼100 µm. The void formation and the relatively large thickness of the metal layer are likely to contribute to the increased series resistance for the solar cells with paste-metallized rear. The upper SEM image in Figure 4(a) shows a zoomed area (marked by a red rectangle in the lower SEM image) of the interface. The upper SEM image shows the PEDOT:PSS layer between silicon and the rear metallization. The thickness of the PEDOT:PSS layer is 170 ± 90 nm.

Unfortunately, the efficiencies of the reference BackPEDOT solar cells with evaporated Ag metal at the rear are relatively low with values of 16.2% and 17.1%, largely due to the very high series resistances of these cells, hinting toward general issues in the cell process which are not related to the rear metallization. The solar cells with paste-metallized rear surface achieve efficiencies of 16.7% and 16.9%. All solar cell efficiencies are relatively moderate, caused by process instabilities, as already mentioned above. Figure 4(b) shows the illuminated J–V curve (red symbols) and J_{sc}–V_{oc} curve (blue symbols) of our best solar cell with low-temperature paste metallization at the rear surface. The insert in Figure 4(b) shows the corresponding solar cell parameters. Our best large-area BackPEDOT solar cell with low-temperature paste rear metallization achieved a short-circuit current density J_{sc} of 36.8 mA cm^{-2}, an open-circuit voltage V_{oc} of 638 mV, a fill factors FF of 72.1% and an efficiency of 16.9%. Importantly, metallization of the PEDOT:PSS layer with low-temperature paste is realized for the first time and leads to results comparable to that of the reference solar cells. These results indicate that the BackPEDOT solar cells can in fact be

Table 2. Illuminated current-voltage and J_{sc}–V_{oc} measurements are performed at the standard testing conditions (25 °C and illumination intensity of 100 mW cm^{-2}).

Rear metallization	J_{sc} [mA cm^{-2}]	V_{oc} [mV]	FF [%]	η [%]	pFF [%]	R_s [Ω cm^2]
Evaporated silver	36.8	636	73.3	17.1	81.8	1.8
Evaporated silver	36.1	630	71.1	16.2	80.9	2.1
Low-temperature metal paste	36.8	638	72.1	16.9	81.6	2.2
Low-temperature metal paste	36.9	644	70.2	16.7	81.6	2.4

Solar cell parameters of the solar cells metallized with evaporated silver and the new low-temperature metal-paste.

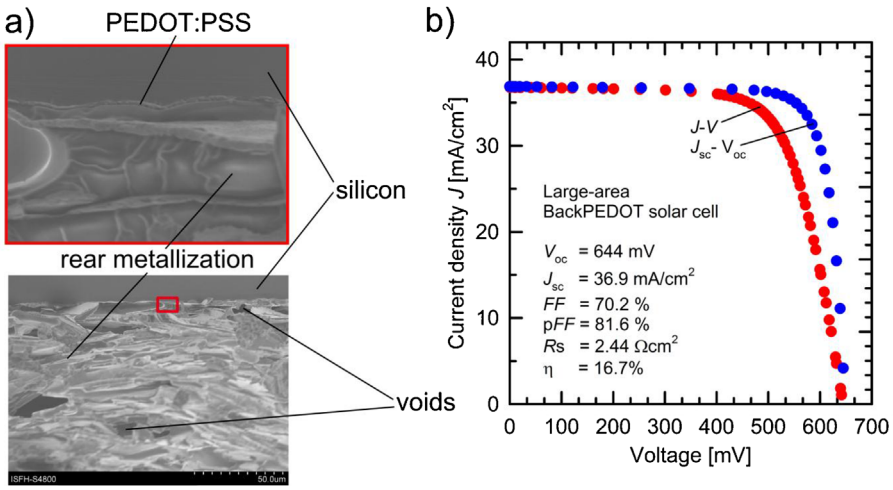

Figure 4. a) Scanning electron microscopy (SEM) image of the silicon/PEDOT:PSS/low-temperature metal paste interface. b) Illuminated J–V curve (red symbols) and J_{sc}–V_{oc} curve (blue symbols) of our best solar cell with low-temperature paste as the rear surface metallization. Corresponding solar cell parameters are shown in the insert.

fully metallized using industrial-type screen-printing technology. However, further optimization of the paste recipe seems to be necessary to allow for thinner and more compact metallization layers at the rear.

3. Conclusion

In conclusion, we have developed a large-area BackPEDOT solar cell with a phosphorus-diffused emitter and a screen-printed Ag grid on the front surface and PEDOT:PSS as hole-collecting and passivating layer at the cell rear. As base material, $15.6 \times 15.6\,cm^2$ industrial-type boron-doped p-type Czochralski-grown silicon wafers were used. We have varied the set-peak temperature from 850 to 870 °C with a total number of 32 solar cells. The optimal set-peak temperature was determined to be 870 °C, resulting in a median solar cell efficiency of 19.2%. Our best BackPEDOT solar cell achieved a short-circuit current density J_{sc} of $38.7\,mA\,cm^{-2}$ and an open-circuit voltage V_{oc} of 656 mV. Based on external quantum efficiency measurements we determined a rear surface recombination velocity $S_{rear} < 70\ cm\,s^{-1}$, which is comparable to today's industrial PERC solar cells. The measured series resistance R_s of $0.63\,\Omega\,cm^2$ proved good hole transport across the PEDOT:PSS/c-Si junction, leading to a fill factors FF of 79.5% and an efficiency of 20.2%. Furthermore, we developed a low-temperature metal paste which is capable to metalize the rear surface of our BackPEDOT solar cells without damaging the rear surface passivation. We demonstrated the principle feasibility of such a low-temperature rear metallization scheme, however, further improvements in the paste recipe seem to be required to allow for the desposition of thinner and more compact metal layers. As one of the fundamental efficicieny-limiting loss mechanisms we have identified parasitic absorption of infrared light within the PEDOT:PSS layer, limiting the short-circuit current densites J_{sc} of our BackPEDOT cells. In first experiments, we have found that adding non-absorbing agents to the PEDOT:PSS dispersion have the potential of increasing the J_{sc} by $1\,mA\,cm^{-2}$. If this improvement in the optical properties can be transferred into the industrial-type BackPEDOT cell, efficiencies exceeding 21% should become possible.

4. Experimental Section

Solar Cells Fabrication Sequence: Standard industrial $15.6 \times 15.6\,cm^2$ pseudo-square 3.2–3.8 Ωcm boron-doped p-type Czochralski-grown (Cz) silicon wafers with an initial thickness of 180 µm were used as base material. After a Puraton cleaning in an ultrasonic bath, the wafers were damage-etched in a potassium hydroxide bath and subsequently RCA-cleaned. After the wafer cleaning, a protection layer was deposited on the rear surface. Next, a random-pyramid (RP) texture was formed in a potassium hydroxide solution on the front surface of the (100)-oriented silicon wafer. After RCA-cleaning an $\sim 80\,\Omega\,sq^{-1}$ n^+ emitter was formed in a quartz-tube furnace (TS 81004, Tempress) in a $POCl_3/O_2$ atmosphere. After phosphorus silicate glass (PSG) removal in an HF dip and a further RCA-cleaning, a PECVD-SiN_x was deposited in a *SiNA* (Meyer Burger) deposition system on the front surface, acting as surface-passivating antireflection coating. Next, a five bus-bar Ag-grid was screen-printed using a DEK screen-printer (DEK Solar Eclipse, ASM Assembly Systems GmbH & Co) on the front surface using a commercial Ag paste. After drying the paste, the wafer was fired in a conveyer-belt furnace. Both, drying and firing were performed in industrial belt furnaces of centrotherm photovoltaics (DO-HTO-5.200-210 and DO-FF-8.600-300, respectively). During the firing sequence, the solar cells were placed on a silicon wafer to reduce the contamination of the silicon bulk. The set-peak temperature (T_{set}) of the firing profile was varied, to deduce the optimal thermal budget. This thermal treatment during firing activates the passivation of the SiN_x layer and forms the contact between Ag paste and the n^+ emitter. The T_{set} values were set at 850, 860, and 870 °C, with a total number of 4 solar cells, 18 solar cells, and 10 solar cells for the specified T_{set}, respectively. After the front surface of the solar cell was finished, the rear protection layer was removed using a 40% HF-diluted solution. To perform this single-side etching, the rear surface of the solar cell was placed on top of an HF-soaked tissue. A constant air flow toward the front surface prevented the parasitic etching of the Ag grid and the SiN_x layer. Next, the PEDOT:PSS dispersion (Clevios™, Heraeus Deutschland GmbH, Leverkusen) was spin-coated in ambient environment onto the

entire rear surface with 500 RPM for 10 s at the first and 1500 RPM for 30 s in the second step, followed by annealing in air at 130 °C for 15 min. Note that in order to achieve a low series resistance, the period between the HF treatment of the silicon surface and PEDOT:PSS deposition has to be as short as possible.[10] Typically, periods of 8–30 min in our cell fabrication were realized. The rear surface was metalized by a 1 µm thick silver layer deposited using e-beam evaporation (BALZERS, BAK 550) or, alternatively, a novel metal paste was printed onto the rear. The low-temperature metal paste was deposited using a 100 µm wire bar (K Hand Coater, RK PrintCoat Instruments Ltd, United Kingdom). After coating the entire PEDOT:PSS surface with the metal paste, the solar cells were dried on a hot-plate at 100 °C for 15 min in air.

Low-Temperature Metal Paste: As a binder Neocryl B-725 dissolved in butyl acetate was used. A total of 100 g of NeoCryl B-725 (DSM Coating resins B.V., Waalwijk, Netherlands) was dissolved in 100 g of butyl acetate (technical grade, VWR International, France) using a roll mixer. As conductive component, silver-coated copper flakes (eConduct Copper 421000, Eckhart GmbH, Hartenstein) with a size of ~40 µm (d_{50}-value) were employed. The silver content of the metal particles is approximately 10%$_{wt}$. A total of 74.25 g eConduct Copper 421000 flakes were wetted with 22.5 g butyl acetate, mixed with a glass rod and 59.4 g of the afore mentioned, highly viscos solution of Neocryl B-725 was added while stirring. As a result, a highly viscos, homogeneous paste was obtained.

Measurement Techniques: The illuminated current-voltage (J–V) and the short-circuit current density – open-circuit voltage (J_{sc}–V_{oc}) characteristics were measured under standard testing conditions (25 °C and illumination intensity of 100 mW cm^{-2}) using a LOANA measurement system (pv-tools, Germany). The electroluminescence, reflectance measurements and spectral response measurements were performed using the integrated characterization tools in the LOANA. The external quantum efficiency of each solar cell, as calculated from the reflectance and spectral response measurements, were used in order to perform a spectral mismatch correction of the short-circuit density J_{sc}. The series resistance R_s was determined based on the measured fill factor FF and the pseudo-fill factor pFF using the equation:

$$FF = pFF\left(1–R_s^* J_{sc}/V_{oc}\right) \quad (1)$$

Scanning electron microscope (SEM) images were recorded using a Hitachi S4800 SEM.

Acknowledgements

The authors acknowledge Ulrike Baumann and Fabian Kiefer of ISFH for screen-printing of the front Ag grid. Priscilla Kochanski is acknowledged for support with the PEDOT:PSS depositions. The work was funded by the German State of Lower Saxony and the German Federal Ministry of Economic Affairs and Energy (BMWi) and by industry partners within the research project "SiPoly" (contract no. 0325884A).

Conflict of Interest

The authors declare no conflict of interest.

Keywords

large-areas, low-temperature pastes, PEDOT:PSS, screen-print, solar cells

Received: November 6, 2017
Published online: February 12, 2018

[1] International Technology Roadmap for Photovoltaics (ITRPV), Frankfurt am Main: VDMA, **2016**.
[2] D. Zielke, A. Pazidis, F. Werner, J. Schmidt, *Sol. Energy Mater. Sol. Cells* **2014**, *131*, 110.
[3] D. Zielke, C. Niehaves, W. Lövenich, A. Elschner, M. Hörteis, J. Schmidt, *Energy Procedia* **2015**, *77*, 331.
[4] S. Avasthi, S. Lee, Y.-L. Loo, J. C. Sturm, *Adv. Mater.* **2011**, *23*, 5762.
[5] L. He, C. Jiang, H. Wang, D. Lai, Rusli, *Appl. Phys. Lett.* **2012**, *100*, 073503.
[6] I. Khatri, T. Imamura, A. Uehara, R. Ishikawa, K. Ueno, H. Shirai, *Phys. Status Solidi C* **2012**, *9*, 2134.
[7] Z. Tang, Q. Liu, I. Khatri, R. Ishikawa, K. Ueno, H. Shirai, *Phys. Status Solidi C* **2012**, *10*, 1.
[8] Q. Liu, M. Ono, Z. Tang, R. Ishikawa, K. Ueno, H. Shirai, *Appl. Phys. Lett.* **2012**, *100*, 183901.
[9] L. He, C. Jiang, H. Wang, H. Lei, D. Lai, Rusli, *Proceedings of the 38th IEEE Photovoltaic Specialists Conference* **2012**, 002785.
[10] R. Gogolin, D. Zielke, W. Lövenich, R. Sauer, J. Schmidt, *Energy Procedia* **2016**, *92*, 638.
[11] J.-Y. Chen, M.-H. Yu, S.-F. Chang, K. W. Sun, *Appl. Phys. Lett.* **2013**, *103*, 133901.
[12] K. A. Nagamatsu, S. Avasthi, J. Jhaveri, J. C. Sturm, *IEEE J. Photovolt.* **2014**, *4*, 260.
[13] Y. Zhang, R. Liu, S. T. Lee, B. Sun, *Appl. Phys. Lett.* **2014**, *104*, 083514.
[14] Y. Zhu, T. Song, F. Zhang, S.-T. Lee, B. Sun, *Appl. Phys. Lett.* **2012**, *102*, 113504.
[15] J. Schmidt, V. Titova, D. Zielke, *Appl. Phys. Lett.* **2013**, *103*, 183901.
[16] S. Avasthi, K. A. Nagamatsu, J. Jhaveri, W. E. McClain, G. Man, A. Kahn, J. Schwartz, S. Wagner, J. C. Sturm, *Proceedings of the 38th IEEE Photovoltaic Specialists Conference* **2014**, 949.
[17] S. Jäckle, M. Liebhaber, J. Niederhausen, M. Büchele, R. Félix, R. G. Wilks, M. Baer, K. Lips, S. H. Christiansen, *ACS Appl. Mater. Interfaces* **2016**, *8*, 8841.
[18] M. Pietsch, S. Jäckle, S. Christiansen, *Appl. Phys. A* **2014**, *115*, 1109.
[19] D. Wang, J. Zhu, L. Ding, P. Gao, X. Pan, J. Sheng, J. Ye, *Jpn. J. Appl. Phys.* **2016**, *55*, 056601.
[20] W. W. He, K. J. Wu, K. Wang, T. F. Shi, L. Wu, S. X. Li, D. Y. Teng, C. Ye, *Sci. Rep.* **2014**, *4*, 3715.
[21] J. He, P. Gao, Z. Yang, J. Yu, W. Yu, Y. Zhang, J. Sheng, J. Ye, J. C. Amine, Y. Cui, *Adv. Mater.* **2017**, *29*, 1606321.
[22] J. Schmidt, D. Zielke, W. Lövenich, M. Hörteis, A. Elschner, *6th World Conference on Photovoltaic Energy Conversion*, **2014**, 869.
[23] R. Gogolin, D. Zielke, A. Descoeudres, M. Despeisse, C. Ballif, J. Schmidt, *Energy Procedia* **2017**, *124*, 593.
[24] K. Bothe, "https://isfh.de/mediathek/software/," ISFH, 09.2017.
[25] R. Brendel, M. Hirsch, R. Plieningerm, J. H. Werner, *IEEE Trans. Electron Devices* **1996**, *43*, 1104.
[26] J. Schmidt, A. Merkle, R. Brendel, B. Hoex, M. C. M. v. d. Sanden, W. M. M. Kessels, *Prog. Photovoltaik. Res. Appl.* **2008**, *16*, 461.
[27] T. Dullweber, J. Schmidt, *IEEE J. Photovolt.* **2016**, *6*, 1366.

